Picosecond-Hetero-FRET Microscopy to Probe Protein-Protein Interactions in Live Cells

Marc Tramier,* Isabelle Gautier,* Tristan Piolot,† Sylvie Ravalet,‡ Klaus Kemnitz,† Jacques Coppey,* Christiane Durieux,* Vincent Mignotte,‡ and Maïté Coppey-Moisan*

*Institut Jacques Monod, UMR 7592, CNRS, Universités P6/P7, 75251 Paris Cedex 05, France; †EuroPhoton GmbH, D-12247, Berlin, Germany; and ‡ICGM, Department of Hematology, Maternité Port-Royal, 75014 Paris, France

ABSTRACT By using a novel time- and space-correlated single-photon counting detector, we show that fluorescence resonance energy transfer (FRET) between cyan fluorescent protein (CFP) and yellow fluorescent protein (YFP) fused to herpes simplex virus thymidine kinase (TK) monomers can be used to reveal homodimerization of TK in the nucleus and cytoplasm of live cells. However, the quantification of energy transfer was limited by the intrinsic biexponential fluorescence decay of the donor CFP (lifetimes of 1.3 ± 0.2 ns and 3.8 ± 0.4 ns) and by the possibility of homodimer formation between two TK-CFP. In contrast, the heterodimerization of the transcriptional factor NF-E2 in the nucleus of live cells was quantified from the analysis of the fluorescence decays of GFP in terms of 1) FRET efficiency between GFP and DsRed chromophores fused to p45 and MafG, respectively, the two subunits of NF-E2 (which corresponds to an interchromophoric distance of 39 ± 1 Å); and 2) fractions of GFP-p45 bound to DsRed-MafG (constant in the nucleus, varying in the range of 20% to 70% from cell to cell). The picosecond resolution of the fluorescence kinetics allowed us to discriminate between very short lifetimes of immature green species of DsRed-MafG and that of GFP-p45 involved in FRET with DsRed-MafG.

INTRODUCTION

Fluorescence resonance energy transfer (FRET) between fluorescent moieties associated with two proteins of interest is a very sensitive method for detecting protein-protein interactions in live cells (Selvin, 2000; Wouters et al., 2001). The availability of mutant variants of the green fluorescent protein (Heim and Tsien, 1996) and of DsRed (Matz et al., 1999) offers a choice of suitable pairs of chromophores that can be covalently linked to a macromolecule of interest. However, owing to the tetramerization of DsRed and to the slow and incomplete maturation process of the chromophore (Baird et al., 2000; Heikal et al., 2000), DsRed has not been often used to tag proteins for FRET studies. Although the most widely used pair of chromophores to detect protein-protein interactions in live cells is CFP/YFP (Pollok and Heim, 1999; Truong and Ikura, 2001), the photophysical properties of these GFP variants have not been studied in detail. In the study of protein-protein interactions by FRET with standard microscopy techniques, a change in the color and/or the fluorescence intensity is commonly interpreted as evidence of energy transfer (Bastiaens et al., 1996; Gordon et al., 1998; Xia and Liu, 2001). However, such changes can be due to specific photophysical properties of these fluorescent proteins, such as photoconversion (Creemers et al., 1999; Malvezzi-Campeggi et al., 2001), photo-induction of a "dark state" (Garcia-Parajo et al., 2000), photobleaching (Patterson et al., 1997), occurrence of other fluorescent species (such as green-emitting immature state of DsRed) (Baird et al., 2000), or other still unknown processes, which cannot be easily monitored by conventional steady-state fluorescence microscopy. In contrast, by using time-correlated single-photon counting to acquire fluorescence decay with few-picosecond resolution, we could study in detail different emitting species, as recently shown for DsRed (Cotlet et al., 2001). For this purpose, we have developed a picosecond time-correlated fluorescence microscopy system that allows us to obtain decay kinetics of extremely low fluorescence coming from a small subcellular volume of a living cell (Gautier et al., 2001; Tramier et al., 2000).

In the present paper we used this technique to compare different fluorescent protein pairs, CFP/YFP and GFP/DsRed, for the study of protein-protein interaction by FRET microscopy in living cells. The thymidine kinase of herpes simplex type 1 virus and the transcriptional factor NF-E2 were taken as model of homodimeric and heterodimeric interactions, respectively. Subunits of these proteic complexes were tagged with different fluorescent protein couples, CFP/YFP and GFP/DsRed. A detailed study of the picosecond fluorescence kinetics of these tagged subunits was carried out with the aim to characterize the fluorescence contributions to specific photophysical states of the fluorescent proteins and to FRET between donor and acceptor for each CFP/YFP and GFP/DsRed pair. In addition, taking advantage of the space-resolved picosecond-fluorescence decay property of the new detector used in the present study, cell to cell variations of bound fraction of donor-tagged subunit were simultaneously carried out in case of the GFP/DsRed pair.

Submitted December 22, 2001, and accepted for publication August 5, 2002.

Address reprint requests to Maïté Coppey-Moisan, Institut Jacques Monod, UMR 7592, CNRS, Universités P6/P7, 2, place Jussieu, 75251 Paris Cedex 05, France. Tel. and Fax: 33-1-44-27-7951; E-mail: maite.coppey@ijm.jussieu.fr.

0006-3495/02/12/3570/08 $2.00

MATERIALS AND METHODS

Construction of fusion proteins

The plasmids encoding the 366-amino acid N-terminal part of TK fused to CFP or YFP, under the control of the TK promoter, was constructed. The pTK14 expression vector for herpes simplex virus type 1 TK was kindly provided by I. Pelletier and F. Colbere-Garapin (Institut Pasteur, Paris, France). CFP and YFP (pECFP-C1 and pEYFP-C1, Clontech, Montigny le Bretonneux, France) were amplified by PCR with an upstream primer (5′-AAAAAAGCGCGCGTGAGCAAGGGCGAGG-3′) and a downstream primer (5′-AAAAAAGCGCGCCTTGTACAGCTCGTCC-3′). The two different PCR products were subcloned in the *BssH*II site of pTK14. The resulting plasmids coded for CFP or YFP were fused to the 366 N-terminal residues ($pTK_{366}CFP$ or $pTK_{366}YFP$) of TK.

A cDNA encoding murine p45 NF-E2 was cloned in frame with GFP in vector pEGFP-C1 (Clontech). This resulted in expression of a fusion protein in which EGFP and p45 are tethered by a linker: TCCGGACTCAGATCTCGAGCTCAAGCTTCGAATTCTTTGTGCTT-GTGGAGACCTGGGGCCATCAGCTGGCACAGTAGG, encoding 26 amino acids.

A cDNA encoding murine MafG was cloned in frame with DsRed in vector pDsRed-C1 (Clontech). This resulted in expression of a fusion protein in which DsRed and MafG are tethered by a linker: CTCAGATCT, encoding three amino acids.

Expression of fusion proteins

Vero and HeLa cells were cultured on glass coverslips in Dulbecco's modified Eagle's medium (Life Technologies, Cergy Pontoise, France), supplemented with fetal calf serum (10%), at 37°C in a 5% CO_2 atmosphere. The cells were transfected with pEGFP-C1, pDsRed-C1, or one of the plasmids encoding TK_{366}-CFP, TK_{366}-YFP, GFP-p45 or DsRed-MafG, or co-transfected with two plasmids encoding recombinant proteins, using FuGENE 6 Transfection Reagent (Roche Molecular Biochemicals, Meylan, France), according to the manufacturer's instructions. Fluorescence (steady-state and time-resolved intensity) were measured two to three days after transfection of the corresponding coding plasmid.

Steady-state fluorescence microscopy

Cells expressing GFP, CFP, YFP, and DsRed fusion proteins were cultured on coverslips that were mounted in a special holder allowing reconstruction of a petri dish and placed on the stage of an inverted microscope (Leica DMIRBE, Leica France, Rueil Malmaison, France). A mercury lamp (50 W) was the excitation source for fluorescence. Cells were imaged through a 100× oil objective (Leica PL Fluotar, NA = 1.3). The fluorescence corresponding to the different tagged proteins was selected using one of the filter set combinations (Omega; Optophotonics, Eaubonne, France): 475AF40 excitation filter/505DRLP dichroic beam splitter/535AF45 emission filter (GFP); 440AF35 excitation filter/460DRLP dichroic beam splitter/480AF30 emission filter (CFP); 480AF30 excitation filter/520DRLP dichroic beam splitter/540AF40 emission filter (YFP) and 535DF35 excitation filter/570DRLP dichroic beam splitter/OG590 emission filter (DsRed). The steady-state fluorescence images were acquired with a cooled slow scan high-resolution (1024 × 1024 pixels) charge-coupled device (CCD) camera (Silar, St Petersburg, Russia) and further processed as described earlier (Coppey-Moisan et al., 1994).

Time domain picosecond fluorescence lifetime microscopy and data analysis

Space-resolved fluorescence lifetimes were obtained by taking advantage of simultaneous acquisition of time and space information on the picosecond time scale by a time- and space-correlated single-photon counting detector (delay-line (DL) detector, EuroPhoton GmbH, Berlin, Germany) (Kemnitz et al., 1997). Space-resolved picosecond fluorescence decays were established by counting and sampling single emitted photons according to 1) the time delay between their arrival and the laser pulse (fluorescence decay by time correlated single photon counting method (O'Connor and Phillips, 1984)); and 2) their coordinate along the detector axis (one-dimensional space-resolution). The microscopy set-up is depicted in Fig. 1. A mode-locked titanium sapphire laser (Millennia 5W/Tsunami 3960-M3BB-UPG kit, Spectra-Physics, Les Ulis, France) was tuned to 880 nm or 960 nm to obtain excitation wavelengths of 440 nm or 480 nm after frequency doubling for CFP and GFP or DsRed chromophores, respectively. The repetition rate was 4 MHz after pulse-picker (Spectra-physics 3980-35). The laser beam was expanded to obtain an illumination field of 80 μm diameter in the object plane with a 100× objective. The optics (objective, dichroic mirrors, and emission filters) were similar to those used for steady-state fluorescence. A galvanometer system, oscillating at 60 Hz, was used to average the interference fringes generated by the passage of the coherent laser beam through the optics of the microscope. The laser power was reduced to 20 nW at the exit of the objective by a neutral density filter placed on the laser beam. A rotating mirror allowed switching between a mercury lamp and laser illumination. A rectangular area of the sample 60 μm long (x-direction) and 5 μm wide was imaged on the sensitive area of the DL detector. The count rate was between 500 and 2000 cps. The 2D multi-channel analyzer combined time- and space-coordinates, which were displayed as a pseudo-color 2D histogram map with 256 and 2048 channels for space and time dimensions, respectively. The acquired fluorescence decays were deconvoluted with the instrument response function and fitted by a Marquardt nonlinear least-square algorithm using Globals Unlimited software (University of Illinois at Urbana-Champaign) with a one- or two-exponential theoretical model, as described elsewhere (Tramier et al., 2000). Fitting procedures were carried out following two different ways: 1) analysis of single decay corresponding to the whole sample and obtained by gathering data over all the space

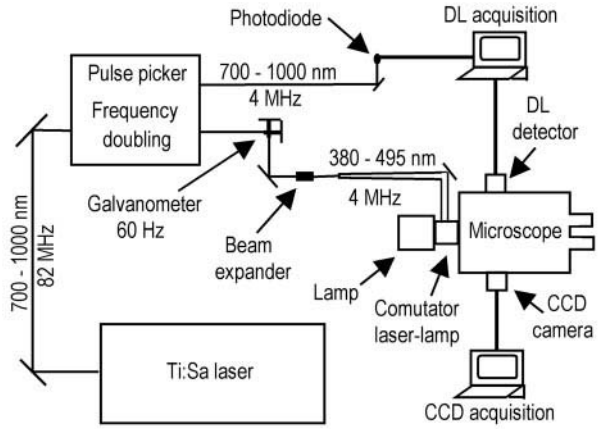

FIGURE 1 Delay line set-up for picosecond fluorescence decay microscopy. A picosecond Ti:Sa laser after pulse picker and frequency doubling delivered 4 MHz repetitive rate pulses at a tunable 380–495 nm wavelength. The fundamental laser rejected from frequency doubling (4 MHz repetitive rate) was used to trigger an ultrafast photodiode (Hamamatsu, Photonics France, Massy, France). The excitation laser beam was transformed by a galvanometer-beam expander system before entering the microscope. A rotating mirror was used as a commutator between lamp and laser excitation. Two outputs of the microscope are used for CCD camera and DL detection. The photodiode signal was used by the DL acquisition to characterize the time difference between the pulse laser and the single photon emission counted by the detector.

channels; and 2) global analysis with or without linked lifetimes over the different decays corresponding to different sample areas and obtained by gathering data over five contiguous space channels.

FRET efficiency (E) was determined by:

$$E = 1 - \tau_{DA}/\tau_D \quad (1)$$

τ_D being the fluorescence lifetime of the donor in the absence of acceptor and τ_{DA} that of the donor in the presence of acceptor at a distance R.

The distance R between the donor and the acceptor was determined from the relation:

$$\tau_{DA} = \tau_D/(1 + (R_0/R)^6) \quad (2)$$

where R_0 is the Förster radius, the distance between the donor and acceptor at which 50% energy transfer takes place.

RESULTS AND DISCUSSION

FRET between CFP and YFP chromophores within the homodimeric protein thymidine kinase of herpes simplex virus

The thymidine kinase (TK) of herpes simplex virus type 1 phosphorylates a wide range of nucleoside analogs. Crystallized in the presence of substrate, TK forms homodimers (Wild et al., 1997), which seem to be the active form (Fetzer et al., 1994). Recently, by using fluorescence anisotropy decay confocal microscopy, which allowed us to unveil FRET between identical GFP chromophores, we have shown that this protein dimerizes in living cells (Gautier et al., 2001). Accordingly, TK was used as a model of homodimeric interactions in living cells.

In this study two unlike chromophores were used as a donor-acceptor couple to measure FRET between TK monomers within the dimer by acquisition of picosecond fluorescence decays of the donor. CFP and YFP were fused to the carboxyl terminus of TK from which the last 10 amino acids were deleted (TK_{366}-CFP and TK_{366}-YFP). Vero cells were either transfected with the expression vector for TK_{366}-CFP or co-transfected with expression vectors for TK_{366}-CFP and TK_{366}-YFP and analyzed 72 h after transfection. In Fig. 2, the fluorescence associated with TK_{366}-CFP expressed alone and with TK_{366}-YFP is shown in panels A and D, respectively. Panel B illustrates the fluorescence associated with TK_{366}-YFP, and panel C an overlay of images B and D. CFP and YFP fluorescence were detected in the cytoplasm and in the nucleus. The CFP molecules in these cells were excited with the pulsed laser, and individual emitted photons were counted according to 1) their coordinate along the detector axis (white rectangle in panels A and D); and 2) the time delay between the laser pulse and the arrival of the emitted photon. The results of photon counting are shown for mono- and co-transfected cells in panels E and G, respectively. Qualitatively, the CFP fluorescence decays were globally faster when TK_{366}-YFP was present, as observed in the 2D normalized histograms (Fig. 2, E and G) as well as in the kinetics of the fluorescence decays collected from the entire channels in each experiment (Fig. 2 F). This can likely be ascribed to FRET from CFP to YFP chromophores within TK_{366}-CFP/TK_{366}-YFP dimers. Analysis of the fluorescence decays yielded lifetimes of 1.29 ± 0.18 ns and 3.96 ± 0.40 ns for TK_{366}-CFP expressed alone and 0.86 ± 0.18 ns and 3.73 ± 0.08 ns for TK_{366}-CFP expressed together with TK_{366}-YFP (Table 1). However, the quantification of the FRET decays is complicated by the fact that the CFP chromophore presents a biexponential decay, as shown for CFP and TK_{366}-CFP proteins (Table 1). The molecular and/or photophysical

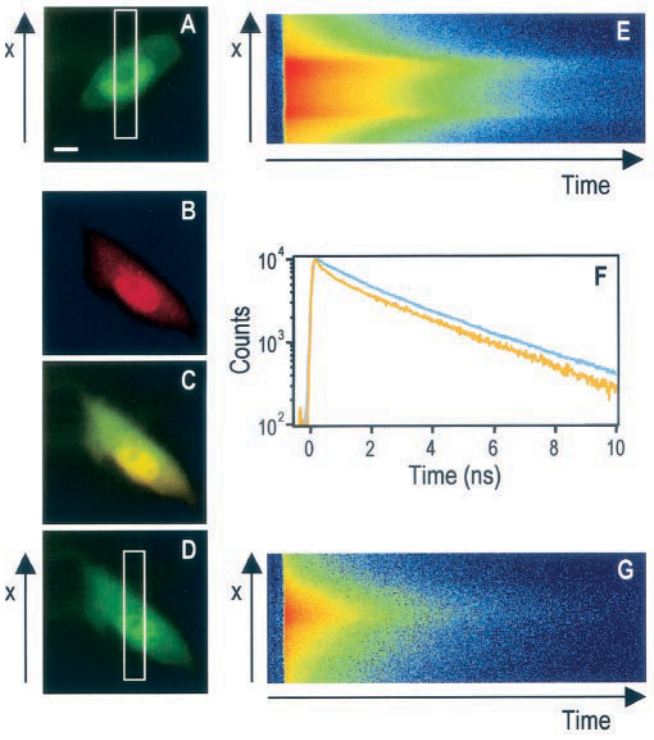

FIGURE 2 FRET determination of the interaction between TK_{366}-CFP and TK_{366}-YFP by picosecond fluorescence decay microscopy. TK_{366}-CFP was expressed or co-expressed with TK_{366}-YFP in Vero cells. Steady-state fluorescence images were acquired with a CCD and using a 50 W high-pressure mercury lamp. (A) Pseudo-color steady-state TK_{366}-CFP image (CFP fluorescence cube) after single-transfection (bar in A = 10 μm). (B) Pseudo-color steady-state TK_{366}-YFP image (YFP fluorescence cube) and (D) Pseudo-color steady-state TK_{366}-CFP image (CFP fluorescence cube) of a co-transfected cell. C is a superposition of B and D. The fluorescence lifetime of CFP was determined using the Ti:Sa laser, tuned to 880 nm (440 nm after doubling) as excitation source and the time- and space-correlated single photon counting DL detector. The white rectangles in A and D represent the region of the sample imaged in the active area of the delay-line detector. (E and G) 2D histograms (*horizontal:* time after laser pulse; *vertical:* space (x-direction) along the delay-line) of single counted photons from CFP fluorescence of TK_{366}-CFP expressed in the absence and presence of TK_{366}-YFP, respectively. F represents the fluorescence decays (*blue* and *orange*) of TK_{366}-CFP (collected from the entire channels along the x-direction) corresponding to the 2D histograms (E and G, respectively). Analysis of these fluorescence decays is presented in Table 1.

TABLE 1 Cyan fluorescence decay kinetic analysis of CFP and CFP-tagged TK_{366} and FRET characterization in living cells

Proteins	Cellular Localization	a_1	τ_1 (ns)	a_2	τ_2 (ns)	$\langle\tau\rangle$ (ns)	n
CFP	Cytoplasm/nucleus	0.53 ± 0.07	1.30 ± 0.22	0.47 ± 0.07	3.84 ± 0.43	2.49 ± 0.18	4
TK_{366}-CFP	Cytoplasm/nucleus	0.54 ± 0.11	1.29 ± 0.18	0.46 ± 0.11	3.96 ± 0.40	2.50 ± 0.12	10
TK_{366}-CFP/TK_{366}-YFP	Cytoplasm/nucleus	0.54 ± 0.06	0.86 ± 0.18	0.46 ± 0.06	3.73 ± 0.08	2.18 ± 0.09	3

a_i is the normalized relative contribution ($\Sigma\ a_i = 1$) of the i fluorescent species characterized by its fluorescence lifetime τ_i, and n is the number of experiments. The error corresponds to the standard deviation. Experiments were carried out 72 h after transfection.

bases for such fluorescence lifetimes have not yet been understood. When all the CFP molecules are not involved in the FRET process, the determination of the intrinsic FRET efficiency is difficult because a four-exponential model should be used to fit the fluorescence decay of TK_{366}-CFP, assuming an equal transfer rate between the two CFP fluorescent species (1.29 ns and 3.96 ns lifetimes) and the acceptor. Moreover, the quantification is even more limited because TK_{366}-CFP can associate as a homodimer. In that case, the transfer taking place between the two identical CFP fluorophores does not change fluorescence lifetime properties. Because of homodimer formation and the complex fluorescence kinetics of CFP, the distance between the CFP and YFP chromophores in the dimer and the fraction of TK_{366}-CFP molecules involved in the FRET process could not be calculated. Nevertheless, by taking the mean fluorescence lifetime of CFP kinetics for TK_{366}-CFP in the absence ($\tau = 2.50$ ns) and in the presence of TK_{366}-YFP ($\tau = 2.18$ ns), an apparent FRET efficiency of 13.3% could be calculated (Eq. 1), indicating the dimerization of TK.

Because of the monoexponential fluorescence decay of GFP (Gautier et al., 2001; Pepperkok et al., 1999; Swaminathan et al., 1996), it seemed that GFP/DsRed might have been a better chromophore pair than CFP/YFP for picosecond-FRET measurements. Unfortunately, TK_{366}-DsRed showed an abnormal cellular localization and aggregation (data not shown), precluding its use.

FRET between GFP and DsRed chromophores within the heterodimeric protein NF-E2

NF-E2 is a heterodimeric member of the basic region-leucine zipper (bZip) class of transcription factors. Its large subunit, called p45 NF-E2, is expressed mainly in two hematopoietic lineages, the erythroid cell lineage (precursor of the red cells) and megakaryocytes (the precursors of blood platelets) (Andrews et al., 1993). p45 associates with a more widely expressed subunit MafG, which is a member of the small-Maf family of proteins (Igarashi et al., 1994). NF-E2 binding sites can be found in a limited number of erythroid (Mignotte et al., 1989; Tugores et al., 1994) and megakaryocytic (Deveaux et al., 1997) genes. In megakaryocytes, MafG is the prevalent small Maf protein (Lecine et al., 1998). We used p45 and MafG as a model of a heterodimeric nuclear protein. The DNA-binding domain of p45 is located at the carboxy-terminal end. We therefore tethered the GFP coding sequence to the coding sequence of the amino-terminus of p45 to generate GFP-p45 fusion cDNA. Similarly, we constructed a DsRed-MafG expression vector. These two vectors were introduced by transfection either separately or together, into HeLa cells, which do not express endogenous p45 or MafG. The green (GFP-p45) and red (DsRed-MafG) fluorescence were both detected in cell nuclei (Fig. 3, *A* and *C*), and co-localized (Fig. 3 *B*), as expected. Picosecond fluorescence decay of GFP-p45 was measured in living cells as described above. The results of photon counting is shown in panel *E* and the decay profile is plotted in panel *D*. From the latter, we observe a biexponential nature of the nuclear GFP-p45 fluorescence decay, the two lifetimes being $\tau_1 = 2.83$ ns and $\tau_2 = 0.74$ ns. Similar lifetime values were found in different experiments (Table 2). Thanks to the spatial correlation of the DL detector, fluorescence decays of GFP-p45 were acquired simultaneously in different locations within the nucleus of this cell, allowing GFP-p45 fluorescence lifetimes and their respective contributions to be determined for different subnuclear areas. The lifetime values of the short component are shown in Fig. 3 *F*. They are between 0.73 and 0.89 ns, the same variation is observed from cell to cell (Table 2). The contribution of each fluorescence component according to the position along the detector axis was evenly distributed within the nucleus (~50% in the cell shown) (Fig. 3 *F*). The longest lifetime value (2.8 ns) corresponds to the typical fluorescence kinetic properties of the GFP chromophore in live cells (Table 2) (Gautier et al., 2001; Pepperkok et al., 1999; Swaminathan et al., 1996). The shortest lifetime value (0.74 ns, Fig. 3) is characteristic of the fluorescence emitted by the GFP chromophore engaged in FRET. This FRET could not be due to a direct molecular interaction between GFP and DsRed of the fusion proteins because the short fluorescence lifetime was not detected when GFP and DsRed were co-expressed (Table 2). By using Eq. 2 and taking $R_0 = 47$ Å (random orientation between GFP-DsRed fluorophores) (Patterson et al., 2000), a decrease of the donor lifetime from 2.82 ± 0.17 ns to 0.90 ± 0.17 ns (Table 2) corresponds to an interchromophoric distance of 39 ± 1 Å.

It was shown that DsRed emits weak green fluorescence before maturation into a red-emitting species in vitro (Baird et al., 2000) as well as in vivo (Terskikh et al., 2000). In

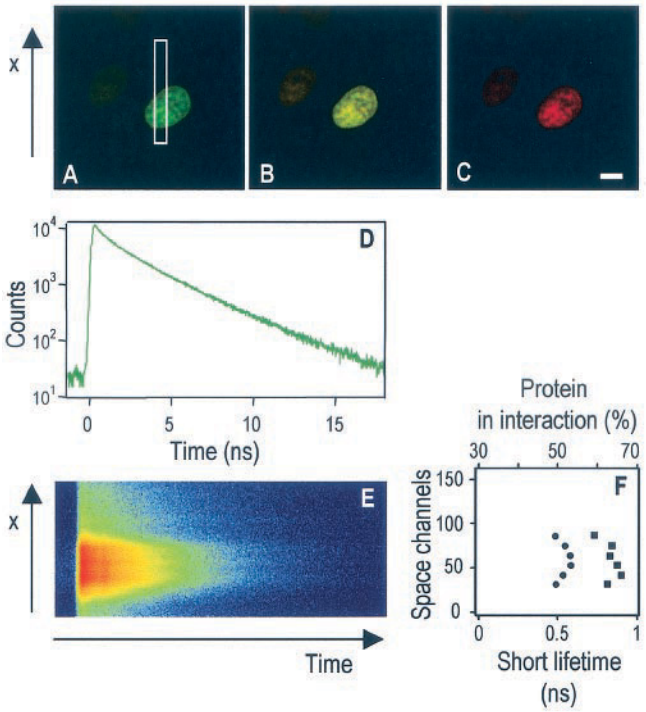

FIGURE 3 FRET determination of the interaction between GFP-p45 and DsRed-MafG by picosecond fluorescence decay microscopy. GFP-P45 and DsRed-MafG were co-expressed in HeLa cells. Steady-state fluorescence images (*A* and *C*) were acquired with a CCD and using a 50 W high-pressure mercury lamp. (*A*) Green fluorescence image (pseudo-color, GFP fluorescence cube) of GFP-p45 of a co-transfected cell; (*C*) Red fluorescence image (pseudo-color, red fluorescence cube) of DsRed-MafG of the same cells than in *A* (bar in $C = 10\ \mu m$). *B* is a superposition of *A* and *C*. GFP fluorescence decays were obtained by using the Ti:Sa laser, tuned to 960 nm (480 nm after doubling) as excitation source and the time- and space-correlated single photon counting DL detector. The white rectangle in *A* represents the region of the sample imaged in the active area of the delay-line detector. (*E*) 2D histogram (*horizontal:* time after laser pulse; *vertical:* space (*x*-direction) along the delay-line) of single counted photons, represented as a pseudo-color image. (*D*) fluorescence decay of GFP-p45 (collected from the entire channel along the *x*-direction). Analysis of this fluorescence decay yielded lifetimes of 2.83 ns (corresponding to unbound GFP-p45) and 0.74 ns (corresponding to GFP-p45 bound to DsRed-MafG). Global analysis using a linked long lifetime (2.83 ns) and a variable short lifetime was carried out. (*F*) Spatial contributions of the percentage of bound GFP-p45 (*circles*) and variations of the short lifetime (*squares*).

addition, DsRed is known to form a tetramer in vitro (Heikal et al., 2000). Therefore, it could be assumed that FRET between the immature green-emitting intermediate of DsRed protein and the matured red-emitting molecule within the tetrameric form of DsRed protein, as demonstrated by two-color excitation single-molecule experiments (Garcia-Parajo et al., 2000), might be the main process giving rise to short green fluorescence lifetime. This possibility could be ruled out, however, due to the following observations:

First, a detailed study of the green emission of DsRed-MafG in living cells has revealed different fluorescent kinetics associated with the green species of DsRed-MafG expressed alone or with GFP-p45. The fast component of 0.90 ± 0.17 ns detected when GFP-p45 was expressed simultaneously to DsRed-MafG could not be found when DsRed-MafG was monotransfected. Indeed, green fluorescence of DsRed-MafG exhibited a three-exponential decay with two main fluorescence lifetimes $\tau_1 = 0.034 \pm 0.051$ ns (80%) and $\tau_2 = 0.51 \pm 0.08$ ns (16%), and a minor one $\tau_3 = 3.23 \pm 0.48$ ns (4%) (standard deviations corresponding to eight cell measurements). Interestingly, in a recent spectroscopic study of immature green DsRed, two short lifetimes (0.026 and 0.12 ns) were found (Cotlet et al., 2001) and attributed to FRET between green- and red-emitting species of DsRed within the tetramer, each corresponding to different oriented chromophores, whereas a longer component (0.47 ns) was associated to tetramers containing only green chromophores. The 0.034 ns and 0.51 ns values likely correspond to FRET from a green chromophore to a red partner, within the DsRed-MafG tetramer, and to the green fluorescence of DsRed-MafG containing only green chromophore, respectively. The component of 3.23 ± 0.48 ns would be associated with the matured red-emitting chromophore, detected in very weak amounts due to the wavelength selection of the emission.

Second, the steady-state intensity of green fluorescence of DsRed-MafG depends critically on the expression level of the protein irrespective of the time after transfection, and could be very low (not shown). Thus, for the determination of GFP-p45/DsRed-MafG interaction, GFP fluorescence decays were acquired from co-transfected cells, where the DsRed-MafG expression level was similar or inferior to that

TABLE 2 Green fluorescence decay kinetic analysis of GFP and GFP-tagged p45 and FRET characterization in living cells

Proteins	Cellular Localization	a_1	τ_1 (ns)	a_2	τ_2 (ns)	R (Å)	n
GFP	Cytoplasm/nucleus	1	2.73 ± 0.05				12
GFP/DsRed	Cytoplasm/nucleus	1	2.58 ± 0.05				6
GFPp45	Nucleus	1	2.68 ± 0.15				4
GFPp45/DsRed-MafG	Nucleus	0.3–0.8	2.82 ± 0.17	0.2 to 0.7	0.90 ± 0.17	39 ± 1	7

a_i is the normalized relative contribution ($\Sigma\ a_i = 1$) of the i fluorescent species characterized by its fluorescence lifetime τ_i. R is the interchromophoric distance between donor and acceptor in the GFP/DsRed FRET couple with a random relative orientation. n is the number of experiments. The error corresponds to the standard deviation.

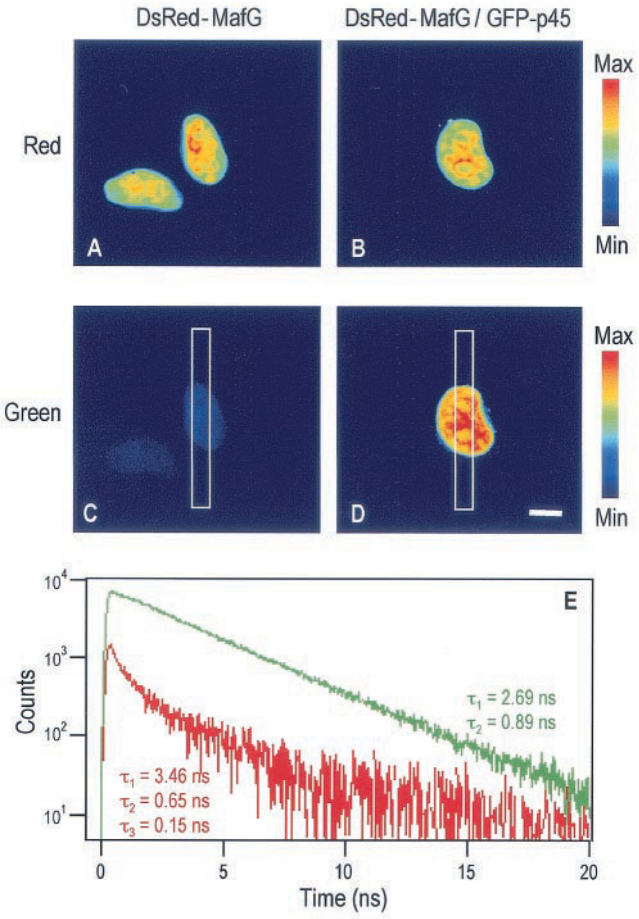

FIGURE 4 Comparison of fluorescence properties (steady-state intensity and kinetics) of the immature green emitting state of DsRed-MafG with those of GFP-p45 in presence of DsRed-MafG. Steady-state intensity images of HeLa cells expressing DsRed-MafG in the red (*A:* OG590 nm long pass) and in the green (*C*: 535AF45 nm bandpass) wavelength range and co-expressing DsRed-MafG and GFP-p45 in the red (*B:* OG590 nm long pass) and in the green (*D:* 535AF45 nm bandpass) wavelength range (bar in $D = 10\ \mu m$). Images displayed in *A* and *B* and in *C* and *D* were acquired under the same conditions, respectively; i.e., excitation intensity (50 W high-pressure mercury lamp) and acquisition time with the CCD. The total red emission intensity from cells displayed in *A* and in *B* were the same (as shown in the pseudo-color display), meaning that the DsRed-MafG expression levels were similar in these two cells. The total green fluorescence of the immature state of DsRed-MafG (*C*) was ~20 times less than the total green fluorescence of GFP-p45 in the presence of the same amount of DsRed-MafG (*D*). Green fluorescence decay (*bottom panel*, *E*) of HeLa cells expressing DsRed-MafG (the red curve corresponds to the photons collected from the white rectangle displayed in *C*) and HeLa cells co-expressing DsRed-MafG and GFP-p45 (the green curve corresponds to the photons collected from the white rectangle displayed in *D*). The green and red decays (*E*) were acquired under the same conditions with the Ti:Sa laser, tuned to 960 nm (480 nm after doubling) and the time- and space-correlated single photon counting DL detector.

of monotransfected DsRed-MafG cells for which the green fluorescence was not significant (Fig. 4 *C*). The comparison of the DsRed-MafG expression level was carried out by measuring the steady-state red fluorescence intensity (excitation with a mercury lamp at 540 nm and emission superior to 590 nm). In Fig. 4 are displayed cells in which DsRed-MafG was expressed at the same level alone (Fig. 4 *A*). or in co-transfection with GFP-p45 (Fig. 4 *B*). The green fluorescence of DsRed-MafG expressed alone was very weak (Fig. 4 *C*) as compared to the total green fluorescence detected after co-transfection of GFP-p45 and DsRed-MafG (Fig. 4 *D*). In addition, the fluorescence decay of the green-emitting species of DsRed (*red curve*) from the white rectangle in Fig. 4 *C* can be fitted with the three characteristic components of immature DsRed-MafG described above. Conversely, the fluorescence decay obtained from the cell co-transfected with GFP-p45 and DsRed-MafG (Fig. 4 *E*, green curve acquired under the same conditions as the red one) could not be fitted with the three components, but with two lifetimes of 2.69 ns and 0.89 ns. This means that the contribution of immature DsRed-MafG in regard to the total green fluorescence was small and not significant in these types of co-transfected cells. Thus, we conclude that the lifetime of 0.90 ± 0.17 ns, observed in GFP-p45 and DsRed-MafG co-expressing cells, was not an artifact due to multimerization of the DsRed moieties coming from the existence of the immature green-emitting state, but could be ascribed to a GFP-p45/DsRed-MafG interaction.

The fraction of GFP-p45 bound to DsRed-MafG is constant within a nucleus (Fig. 3 *F*) but varies from cell to cell (Table 2). Simultaneous acquisitions of fluorescence decays of GFP-p45 after co-transfection with DsRed-MafG from the three cells imaged in Fig. 5 *C* are displayed in Fig. 5 *E*. The differences shown on the normalized fluorescence decays (Fig. 5 *D*) corresponding to the decays of positions 1, 2, and 3 along the sensitive area of the detector arise from different values of the preexponential factor of the short component. The fraction of GFP-p45 bound to DsRed-MafG was thus determined to be 30% in the two lower cells (positions 2 and 3) and 24% in the upper cell (position 1) (Fig. 5 *F*). Thus, the weakest steady-state fluorescence in the upper cell was not due to a higher FRET efficiency or bound fraction of GFP-p45, but likely to a smaller GFP-p45 expression level than in the two other cells in Fig. 5. This result could be obtained owing to the information contained in the full picosecond time-resolved fluorescence decay.

CONCLUSIONS

FRET measurement provides a useful tool to detect interactions between fluorescent tagged proteins and is now used to follow the dynamics of interactions between specific proteins in relation to biological processes directly in the live cell (Li et al., 2001; Mochizuki et al., 2001; van der Wal et al., 2001; Verveer et al., 2000). However, the determination and the quantification of FRET are difficult tasks to carry out under the microscope when the stoichiometry of the donor-acceptor pair cannot be ensured. Picosecond time- and space-correlated single-photon counting methods

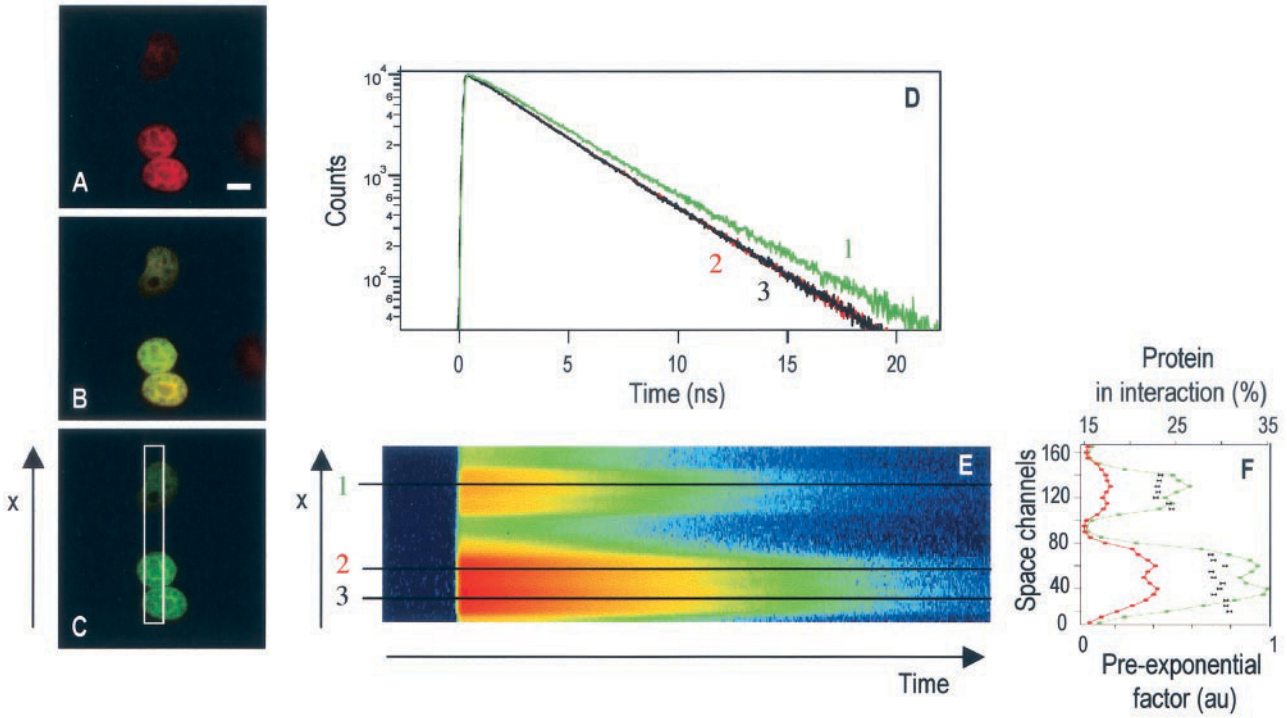

FIGURE 5 Cell-to-cell variations of the proportion of GFP-p45 in interaction with DsRed-MafG. Steady-state fluorescence intensity of HeLa cells co-expressing DsRed-MafG and GFP-p45 in the red (*A:* OG590 nm long pass, pseudo-color) and in the green (*C:* 535AF45 nm bandpass, pseudo-color) wavelength range (bar in $A = 10\ \mu m$). (*B*) Superposition of *A* and *C*. The white rectangle in *C* represents the region of the sample imaged in the active area of the delay-line detector. (*D*) Fluorescence decays of green fluorescence corresponding to space channels at positions 1, 2, and 3 (binning of 5 channels). Global analysis of the fluorescence decays (binning of 5 channels) with linked lifetimes gives the variation of preexponential amplitude of short and long fluorescence lifetime components along space channels. (*E*) 2D histogram of single counted photons collected from the white rectangle in *C*, represented as a pseudo-color image. (*F*) Spatial contribution of the preexponential amplitude of space-associated decay (*green:* 2.63 ns; *red:* 0.90 ns) and of the percentage of GFP-p45 in interaction with DsRed-MafG (*black*).

in microscopy present several advantages for quantification of FRET microscopy in living cells, such as the direct determination of 1) intrinsic FRET efficiency; 2) several lifetimes, even close ones; and 3) the ratio of bound proteins in different subcellular locations. The very high sensitivity of this technique allows extremely low excitation intensity to be used, avoiding photobleaching, and very low levels of fluorescent proteins to be detected.

The possibility to carry out FRET in living cells relies on the existence of GFP variants and, more recently, of the red fluorescent protein DsRed, exhibiting different spectral properties that provided several donor-acceptor pairs (Patterson et al., 2000). Measuring fluorescence decay kinetics in the picosecond range appears to be a way to circumvent some of the difficulties encountered with DsRed (complex maturation process). The single-exponential fluorescence decay of the GFP chromophore (Gautier et al., 2001; Pepperkok et al., 1999; Swaminathan et al., 1996) makes the GFP-DsRed combination a suitable pair for picosecond-FRET microscopy. However, if the protein fused with DsRed aggregates, the CFP-YFP pair, despite the biexponential fluorescence decay exhibited by CFP, can be used. Indeed, with this pair, measurement of FRET efficiency is difficult, but protein-protein interaction can be unveiled, as it has been shown here, with the dimerization of TK_{366}-CFP/TK_{366}-YFP. For homodimer formation, the characterization of FRET between unlike chromophores is made difficult by the mixture of donor-donor and donor-acceptor dimers. In such cases, the molecular parameters of the dimer can be defined by fluorescence anisotropy decay to measure FRET between like chromophores, as shown previously (Gautier et al., 2001). Taken together, these picosecond time-resolved microscopies are unsurpassed techniques for studying protein-protein interactions as a function of time and space in living cells.

We are indebted to Dr. Richard D'Ari, Dr. Marie-Jo Masse, and Dr. Daniele Sanvitto for critical reading of the manuscript.

This work was supported by European Union Grant BIO4 CT97 2177; the Association pour la Recherche sur le Cancer Grants 9222 and 5632 (to J.C.) and 9518 and 5936 (to V.M.); the Groupement des Entreprises Françaises de Lutte contre le Cancer Grant 586108 (to C.D.); and the laboratory Glaxo Wellcome and the region Iles-de-France (SESAME). M. Tramier was supported by the Ligue Nationale Contre le Cancer and also, as well as T. Piolot, by a European Union fellowship.

REFERENCES

Andrews, N. C., H. Erdjument-Bromage, M. B. Davidson, P. Tempst, and S. H. Orkin. 1993. Erythroid transcription factor NF-E2 is a haematopoietic-specific basic-leucine zipper protein. *Nature.* 362:722–728.

Baird, G. S., D. A. Zacharias, and R. Y. Tsien. 2000. Biochemistry, mutagenesis, and oligomerization of DsRed, a red fluorescent protein from coral. *Proc. Natl. Acad. Sci. U.S.A.* 97:11984–11989.

Bastiaens, P. I. H., I. V. Majoul, P. J. Verveer, H. D. Soeling, and T. M. Jovin. 1996. Imaging the intracellular trafficking and state of the AB5 quaternary structure of cholera toxin. *EMBO J.* 15:4246–4253.

Coppey-Moisan, M., J. Delic, H. Magdelenat, and J. Coppey. 1994. Principle of digital imaging microscopy. *Methods Mol. Biol.* 33:359–393.

Cotlet, M., J. Hofkens, S. Habuchi, G. Dirix, M. van Guyse, J. Michiels, J. Vanderleyden, and F. C. de Schryver. 2001. Identification of different emitting species in the red fluorescent protein DsRed by means of ensemble and single-molecule spectroscopy. *Proc. Natl. Acad. Sci. U.S.A.* 98:14398–14403.

Creemers, T. M. H., A. J. Lock, V. Subramaniam, T. M. Jovin, and S. Völker. 1999. Three photoconvertible forms of green fluorescent protein identified by spectral hole-burning. *Nat. Struct. Biol.* 6:557–560.

Deveaux, S., S. Cohen-Kaminsky, R. A. Shivdasani, N. C. Andrews, A. Filipe, I. Kuzniak, S. H. Orkin, P. H. Romeo, and V. Mignotte. 1997. p45 NF-E2 regulates expression of thromboxane synthase in megakaryocytes. *EMBO J.* 16:5654–5661.

Fetzer, J., M. Michael, T. Bohner, R. Hofbauer, and G. Folkers. 1994. A fast method for obtaining highly pure recombinant herpes simplex virus type 1 thymidine kinase. *Protein Expr. Purif.* 5:432–441.

Garcia-Parajo, M. F., G. M. J. Segers-Nolten, J. A. Veerman, J. Greve, and N. F. van Hulst. 2000. Real-time light-driven dynamics of the fluorescence emission in single green fluorescent protein molecules. *Proc. Natl. Acad. Sci. U.S.A.* 97:7237–7242.

Gautier, I., M. Tramier, C. Durieux, J. Coppey, R. B. Pansu, J.-C. Nicolas, K. Kemnitz, and M. Coppey-Moisan. 2001. Homo-FRET microscopy in living cells to measure monomer-dimer transition of GFP-tagged proteins. *Biophys. J.* 80:3000–3008.

Gordon, G. W., G. Berry, X. H. Liang, B. Levine, and B. Herman. 1998. Quantitative fluorescence resonance energy transfer measurements using fluorescence microscopy. *Biophys. J.* 74:2702–2713.

Heikal, A. A., S. T. Hess, G. S. Baird, R. Y. Tsien, and W. W. Webb. 2000. Molecular spectroscopy and dynamics of intrinsically fluorescent proteins: coral red (DsRed) and yellow (Citrine). *Proc. Natl. Acad. Sci. U.S.A.* 97:11996–12001.

Heim, R., and R. Y. Tsien. 1996. Engineering green fluorescent protein for improved brightness, longer wavelengths and fluorescence resonance energy transfer. *Curr. Biol.* 6:178–182.

Igarashi, K., K. Kataoka, K. Itoh, N. Hayashi, M. Nishizawa, and M. Yamamoto. 1994. Regulation of transcription by dimerization of erythroid factor NF-E2 p45 with small Maf proteins. *Nature.* 367:568–572.

Kemnitz, K., L. Pfeifer, R. Paul, and M. Coppey-Moisan. 1997. Novel detectors for fluorescence lifetime imaging on the picosecond time scale. *J. Fluo.* 7:93–98.

Lecine, P., V. Blank, and R. A. Shivdasani. 1998. Characterization of the hematopoietic transcription factor NF-E2 in primary murine megakaryocytes. *J. Biol. Chem.* 273:7572–7578.

Li, H. Y., E. K. Ng, S. M. Lee, M. Kotaka, S. K. Tsui, C. Y. Lee, K. P. Fung, and M. M. Waye. 2001. Protein-protein intercation of FHL3 with FHL2 and visualization of their interaction by green fluorescent proteins (GFP) two-fusion fluorescence resonance energy transfer (FRET). *J. Cell. Biol.* 80:293–303.

Malvezzi-Campeggi, F., M. Jahnz, K. G. Heinze, P. Dittrich, and P. Schwille. 2001. Light-induced flickering of DsRed provides evidence for distinct and interconvertible fluorescent states. *Biophys. J.* 81: 1776–1785.

Matz, M. V., A. F. Fradkov, Y. A. Labas, A. P. Savitsky, A. G. Zaraisky, M. L. Markelov, and S. A. Lukyanov. 1999. Fluorescent proteins from nonbioluminescent Anthozoa species. *Nat. Biotechnol.* 17:969–973.

Mignotte, V., J. F. Eleouet, N. Raich, and P. H. Romeo. 1989. Cis- and trans-acting elements involved in the regulation of the erythroid promoter of the human porphobilinogen deaminase gene. *Proc. Natl. Acad. Sci. U.S.A.* 86:6548–6552.

Mochizuki, N., S. Yamashita, K. Kurokawa, Y. Ohba, T. Nagai, A. Miyawaki, and M. Matsuda. 2001. Spatio-temporal images of growth-factor-induced activation of Ras and Rap1. *Nature* 411:1065–1068.

O'Connor, D. V., and D. Phillips. 1984. Time-Correlated Single Photon Counting. Academic Press, New York.

Patterson, G. H., S. M. Knobel, W. D. Sharif, S. R. Kain, and D. W. Piston. 1997. Use of the green fluorescent protein and its mutants in quantitative fluorescence microscopy. *Biophys. J.* 73:2782–2790.

Patterson, G. H., D. W. Piston, and B. G. Barisas. 2000. Förster distances between green fluorescent protein pairs. *Anal. Biochem.* 284:438–440.

Pepperkok, R., A. Squire, S. Geley, and P. I. Bastiaens. 1999. Simultaneous detection of multiple green fluorescent proteins in live cells by fluorescence lifetime imaging microscopy. *Curr. Biol.* 9:269–272.

Pollok, B. A., and R. Heim. 1999. Using GFP in FRET-based applications. *Trends Cell Biol.* 9:57–60.

Selvin, P. R. 2000. The renaissance of fluorescence resonance energy transfer. *Nat. Struct. Biol.* 7:730–734.

Swaminathan, R., S. Bicknese, N. Periasamy, and A. S. Verkman. 1996. Cytoplasmic viscosity near the cell plasma membrane: translational diffusion of a small fluorescent solute measured by total internal reflection-fluorescence photobleaching recovery. *Biophys. J.* 71:1140–1151.

Terskikh, A., A. Fradkov, G. Ermakova, A. Zaraisky, P. Tan, A. V. Kajava, X. Zhao, S. Lukyanov, M. Matz, S. Kim, I. Weissman, and P. Siebert. 2000. Fluorescent timer: protein that changes color with time. *Science.* 290:1585–1588.

Tramier, M., K. Kemnitz, C. Durieux, J. Coppey, P. Denjean, R. B. Pansu, and M. Coppey-Moisan. 2000. Restrained torsional dynamics of nuclear DNA in living proliferative mammalian cells. *Biophys. J.* 78: 2614–2627.

Truong, K., and M. Ikura. 2001. The use of FRET imaging microscopy to detect protein-protein interactions and protein conformational changes in vivo. *Curr. Opin. Struct. Biol.* 11:573–578.

Tugores, A., S. T. Magness, and D. A. Brenner. 1994. A single promoter directs both housekeeping and erythroid preferential expression of the human ferrochelatase gene. *J. Biol. Chem.* 269:30789–30797.

van der Wal, J., R. Habets, P. Varnai, T. Balla, and K. Jalink. 2001. Monitoring agonist-induced phospholipase C activation in live cells by fluorescence resonance energy transfer. *J. Biol. Chem.* 276: 15337–15344.

Verveer, P. J., F. S. Wouters, A. R. Reynolds, and P. I. Bastiaens. 2000. Quantitative imaging of lateral ErbB1 receptor signal propagation in the plasma membrane. *Science.* 290:1567–1570.

Wild, K., T. Bohner, G. Folkers, and G. E. Schulz. 1997. The structures of thymidine kinase from herpes simplex virus type 1 in complex with substrates and a substrate analogue. *Protein Sci.* 6:2097–2106.

Wouters, F. S., P. J. Verveer, and P. I. H. Bastiaens. 2001. Imaging biochemistry inside cells. *Trends Cell Biol.* 11:203–211.

Xia, Z., and Y. Liu. 2001. Reliable and global measurement of fluorescence resonance energy transfer using fluorescence microscopes. *Biophys. J.* 81:2395–2402.